Key Engineering Materials
ISSN: 1662-9795, Vol. 1055, pp 93-98
doi:10.4028/p-VQop5J

Submitted: 2025-09-08
Revised: 2025-12-15
Accepted: 2026-02-26
Online: 2026-05-19

Study of SiC Thyristors with Integrated Temperature Sensors

Shuhao Cheng[1,a*], Kaiyu Chen[2,b], Zihan Zhang[1,c], Xiaowen Wang[2,d], Lei Yuan[1,e*], Da Huo[1,f], Xuesong Liu[3,g], Tongxiao Hou[3,h], Renxu Jia[1,i], Yuming Zhang[1,j]

[1]Faculty of Integrated Circuit, Xidian University, Xi'an 710071, China

[2]Alkaidsemi Electronic Technology Ltd., Shanghai, China

[3]Beijing BJAST Holdings Co., Ltd., Beijing, China

[a]13757758666@163.com, [b]gary_chen@alkaidsemi.com, [c]24251111422@stu.xidian.edu.cn, [d]xiaowen_wang@alkaidsemi.com, [e]yuanlei@xidian.edu.cn, [f]22111213858@stu.xidian.edu.cn, [g]lxs6721@126.com, [h]644988605@qq.com, [i]rxjia@mail.xidian.edu.cn, [j]zhangym@xidian.edu.cn

Keywords: 4H-SiC GTO, PiN diode, Temperature sensor, Real-time temperature monitoring.

Abstract. SiC GTOs, with high current handling capability, are promising for high-voltage and high-power applications, but they also have temperature-related reliability issues, so real-time junction temperature monitoring is needed. In this paper, a novel 4H-SiC gate turn-off thyristor (GTO) structure with integrated temperature sensor is proposed. The proposed sensor is compatible with the SiC GTO process and allows for real-time temperature monitoring. TCAD simulation results show that the integrated sensor has a high sensitivity of 1.64mV/K and linearity of 0.99891, the temperature sensor monitors the internal temperature of the GTO device in real time with an error of no more than 2 K during complete GTO switching. This new structure is conducive to enhancing the reliability of SiC thyristor applications and system miniaturization.

Introduction

Gate turn-off thyristors (GTOs) are high-power semiconductor devices commonly used in applications such as power converters, inverters, and pulsed power switches. They serve as key components in wind power systems to stabilize output power and current [1], and are widely employed in high-speed railways and high-voltage direct current (HVDC) transmission [2]. However, conventional silicon (Si) GTOs are constrained by the material's theoretical limits, which are inadequate for modern high-voltage systems. To address these limitations, silicon carbide (SiC) has emerged as a promising third-generation semiconductor material due to its wide bandgap, high thermal conductivity, and high saturation carrier velocity, leading to significant research interest in SiC-based GTOs for their superior current capability, high blocking voltage, and high-temperature and high-frequency operation.

Despite these benefits, SiC GTOs also present several reliability challenges, most of which are temperature-related [3-5]. It is evident that, under high-voltage and high-current switching conditions, effective thermal management is essential to prevent junction overheating. Thermal failure occurs when the junction temperature exceeds safe limits. Therefore, real-time temperature monitoring is essential, and since conventional physical methods are prone to inaccuracy and delay, integrated temperature sensors represent a promising direction for future developments.

Recent developments in SiC temperature sensors include PN junctions, PiN transistors, Schottky barrier diodes (SBDs), and body resistors. Among these, SiC PiN diode-based sensors exhibit high sensitivity (4.3 mV/°C) and excellent linearity (0.9996) from room temperature up to 460°C [6]. The low temperature dependence of the saturation current Is*Is* contributes to improved linearity. Additionally, a PTAT (Proportional to Absolute Temperature) structure using the voltage difference between two SiC PiN diodes can eliminate the influence of series resistance [7].

In this paper, a novel SiC GTO structure with an integrated temperature sensor is designed and investigated, offering advantages in process compatibility and compact layout. The paper first introduces the structure and operational principle of the proposed device. followed by an analysis of

the temperature sensor's linearity and sensitivity. Finally, the switching characteristics of the integrated SiC GTO are simulated, and the carrier behavior, temperature distribution, and dynamic temperature measurement process are examined across different operational phases, demonstrating its capability for real-time thermal monitoring.

Device Structure

In order to study the operation of the device during the switching process and to obtain the carrier and temperature distribution inside the device, the device structure was modeled using TCAD software. It should be noted that the 2D simulation simplifies the actual three-dimensional heat transfer; therefore, the following thermal and sensor response results are intended for qualitative analysis of trends and operational principles, rather than as quantitatively precise predictions. Fig. 1 shows the device cross-section of the integrated temperature sensor GTO. Terminal structures are generated by ion implantation at the same time as the gate ohmic contact region after the P-drift region etching is completed, which has a width of 8μm, an injection depth of 1μm and a doping concentration of $2\times10^{17}cm^{-3}$, this terminal structure also serves as an isolation area for the temperature sensors at the same time. N+ substrate doping concentration of $1\times 10^{19}cm^{-3}$. The thickness of the P-buffer layer was 2μm and the doping concentration was $2\times10^{17}cm^{-3}$. The thickness of the P-drift region was 30μm and the doping concentration was $3\times10^{15}cm^{-3}$. The thickness of the N-base region was 3μm and the doping concentration was $2\times10^{17}cm^{-3}$. The thickness of the P+ Anode region was 2μm and the doping concentration was $1\times10^{19}cm^{-3}$.

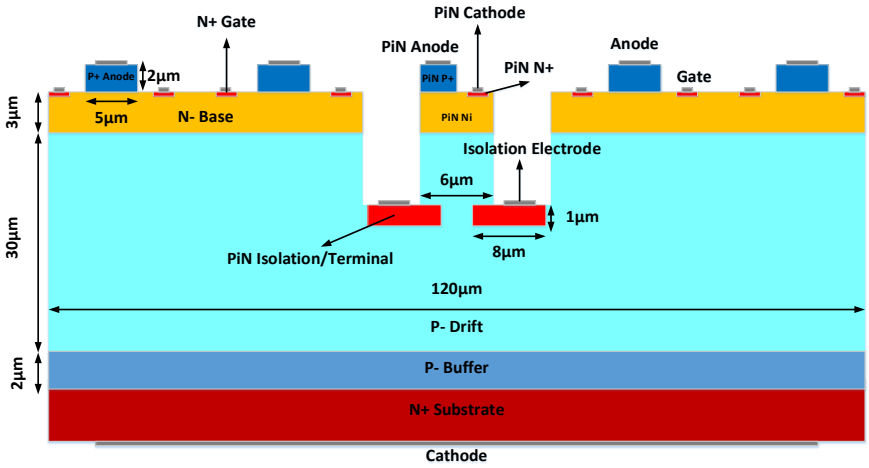

Fig. 1. 4H-SiC GTO Integrated Temperature Sensor Structure.

The physical models used in the simulation process include: Shockley-Read-Hall recombination model, Auger recombination model, IncompleteIonization model, DopingDependence model, HighFieldSaturation model, BandGapNarrowing model, thermodynamic model [8-12].

Results and Discussion

Fig. 2 illustrates the current–voltage characteristics of the temperature sensor measured at different temperatures. The relationship between current and voltage follows Eq. 1 while $qV_d >> \eta kT$:

$$V_d = \frac{\eta kT}{q}\ln\left(\frac{I_d}{I_s}\right) \tag{1}$$

where η is the ideality factor, I_s is the saturation current, and k is the Boltzmann constant. At low sensor currents, the voltage drop decreases as temperature increases, primarily due to the enhanced conductance modulation effect. Conversely, at high sensor currents, the influence of temperature on carrier mobility becomes dominant, leading to an increase in the sensor voltage drop with rising temperature.

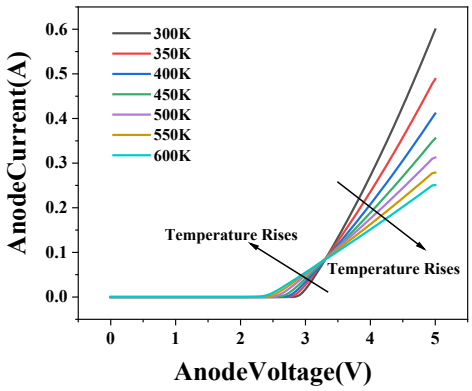

Fig. 2. I-V Characteristics of sensors at different temperature.

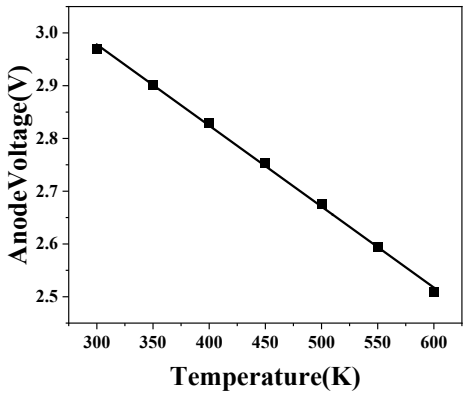

Fig. 3. V-T Characteristics of Temperature Sensors.

Fig. 3 shows the relationship between the temperature sensor voltage drop and temperature for a certain operating current I_d. When the effect of temperature on the ideal factor and saturation current is not taken into account, there is an approximately linear relationship between the voltage drop V_d and the temperature.

Temperature sensors integrated on the GTO need to be compatible with the GTO process, the doping concentration, thickness and other parameters need to be kept constant, and only the operating current can be changed to adjust the linearity and sensitivity of two parameters. Sensitivity and linearity(R^2) are two important parameters of temperature sensors that reflect their ability to monitor temperature.

The V-T characteristics of the sensors with different operating currents and the relationship between operating current and sensor sensitivity and linearity are shown in Fig. 4.

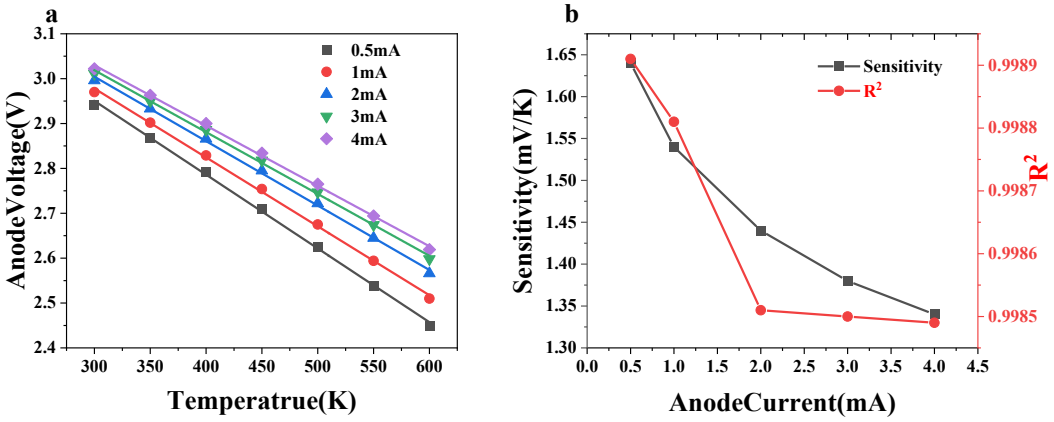

Fig. 4. (a) Sensor V-T characteristics at different currents;(b) Relationship between sensor sensitivity and linearity at different currents.

From Fig. 4(b), it can be seen that the linearity and sensitivity of the sensor decreases with increasing operating current, The reason is that as the operating current increases the on-resistance of the sensor decreases and the reverse saturation current increases.

The integrated PiN temperature sensor has lower linearity and sensitivity parameters compared to the longitudinal PiN temperature sensor in [6] because of the need for compatibility with the GTO process. However, the sensitivity of the Schottky diode is 1.21mV/K compared to the Schottky diode sensor integrated in SiC MOS in [13] at the same operating current, whereas the sensitivity of the integrated PiN temperature sensor is better than the Schottky diode sensor at 1.54mV/K. It also has an advantage over Schottky diode temperature sensors with a maximum sensitivity of 1.18 mV/K as mentioned in [14].

Simulation of an Integrated Temperature Sensor GTO Using Switching Circuits, Fig. 5 shows the switching characteristic test circuit of SiC GTO. The circuit system includes resistors R_1 and R_2, a GTO thyristor, a voltage source V_2 and a current source I_1 that generates a gate trigger signal.

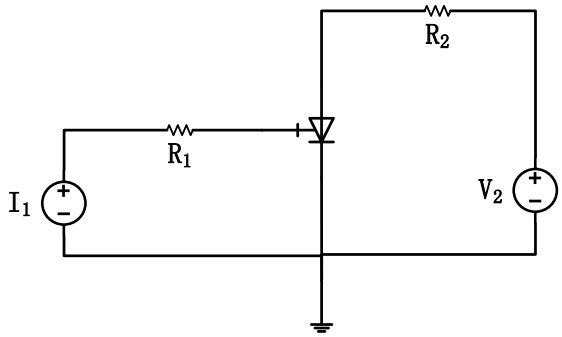

Fig. 5. Thyristor Switching Characteristics Simulation Circuit.

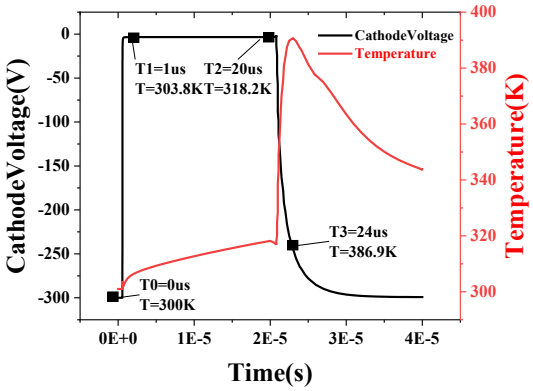

Fig. 6. GTO temperature change during switching.

While making the switching circuit connections to the GTO, a current source is also required to connect the temperature sensor, which operating current is set to 1mA. The temperature variations during the switching process are shown in Fig. 6, and four time points during the switching process are selected to analyze the carrier distribution, the actual temperature of the device, the sensor detection temperature distribution.

During the switching process the thyristor experiences a complete operating state. At first a negative voltage is applied to the cathode and the device is in the blocking state, then a negative signal is applied to the gate and the device changes from the blocking state to the on state. Fig. 7 shows the temperature and carrier distribution before and after the GTO is turned on from T0 to T1.

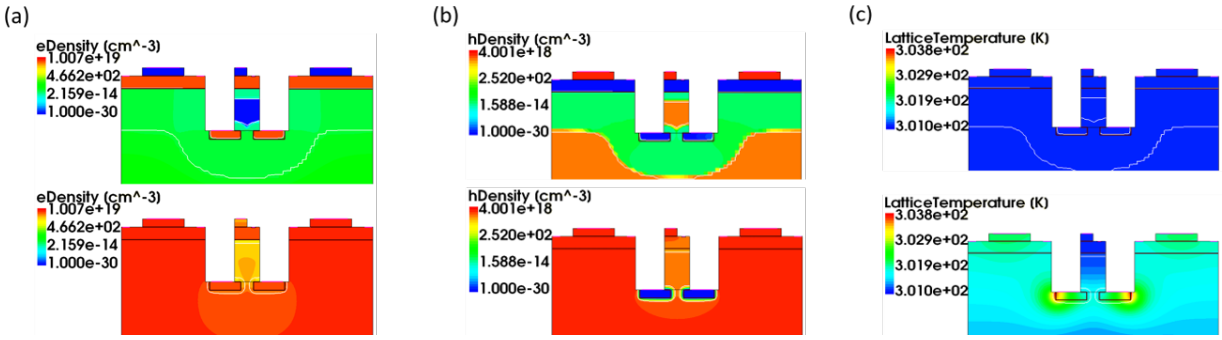

Fig. 7. (a) Electron density (b) Hole density (c) Temperature distribution during device turn-on.

From the carrier distribution in Fig. 7, it can be seen that holes in the P+ anode region and electrons in the N+ substrate region arrive at the P-drift region during device turn-on to undergo conductance modulation to make the device voltage drop. From the distribution of holes, the PN junction formed by the N-base region and the P-drift region changes from reverse bias to forward bias, the device conducts, and the isolation region formed by the terminal structure can play a good role in isolation. Temperature changes during opening occur mainly in the isolated area of the sensor which are minimal.

The carrier distribution remains stable after GTO conducting. Temperature changes occur in the isolation zone are small at around 10K， Fig. 8 shows the carrier and temperature distribution of the GTO during conduction from T1 to T2.

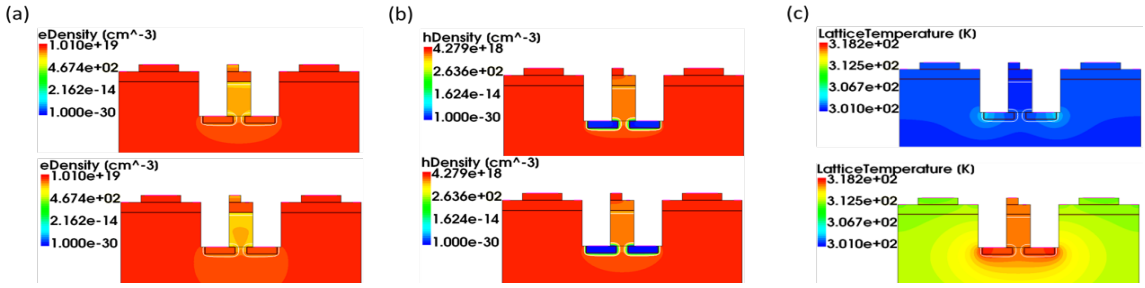

Fig. 8. (a) Electron density (b) Hole density (c) Temperature distribution during device conduction.

During the change of the device from conducting to blocking, a positive signal needs to be applied to the gate to compound and extract the carriers in the drift region, The carrier and temperature distribution from T2 to T3 during turn-off is shown in Fig. 9.

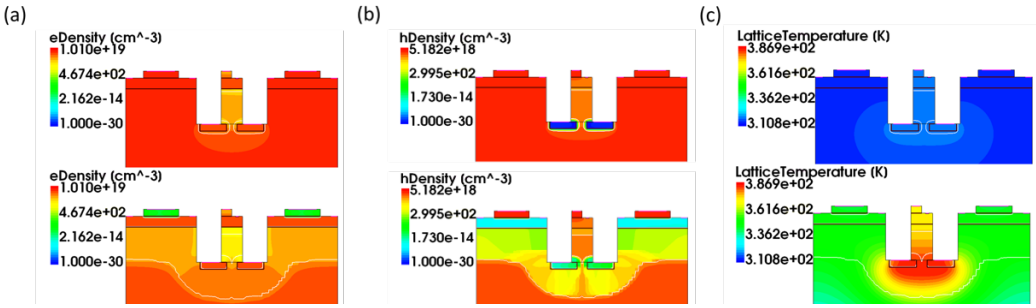

Fig. 9. (a) Electron density (b) Hole density (c) Temperature distribution during device turn-off.

Carrier concentration in the drift region during turn-off decreases with gate extraction, The conductivity of the drift region decreases and the PN junction formed by the N-base and P-drift regions is reversely biased as seen from the distribution of holes, the device voltage drop increases. The temperature of the device varies greatly due to the high current and voltage to be withstood during turn-off.

During the switching simulation of the integrated temperature sensor GTO, the operating current of the sensor is constant at 1mA and the variation of the sensor's voltage drop with time is shown in Fig. 10.

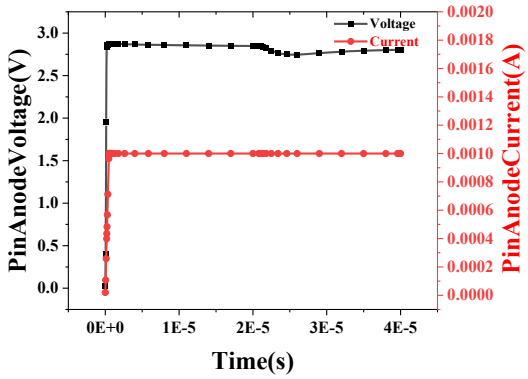

Fig. 10. Sensor current and voltage over time.

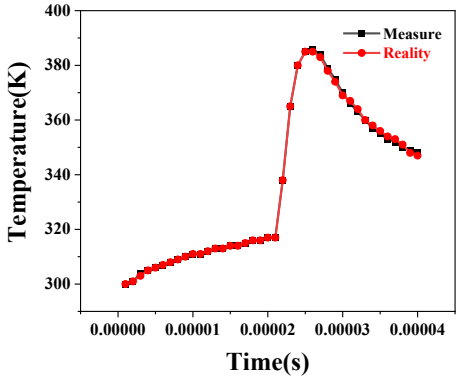

Fig. 11. Comparison of sensor measurements with actual device temperature.

In Fig. 10, as the sensor current stable, its voltage also remains stable. The voltage varies with the temperature of the integrated sensor, due to the large temperature change during turn-off, the sensor voltage change during turn-off is also more pronounced.

Based on the voltage response of the sensor shown in Fig. 10 and the previously established V–T relationship from Fig. 3, the temperature extracted from the sensor closely matches the actual device temperature. As illustrated in the real-time monitoring results in Fig. 11, during the turn-on phase under low operating voltage, both the actual temperature change and the sensor voltage drop are minimal, leading to only a slight detected temperature variation. In contrast, the turn-off transition

subjects the device to high voltage and current, causing significant heating reflected by a sharp decrease in sensor voltage and a corresponding large temperature rise, with the peak temperature occurring during turn-off. After turn-off, as the device cools due to reduced current, the sensor voltage increases and the detected temperature declines. Throughout the entire process, the sensor demonstrates high accuracy in tracking device temperature, with errors not exceeding 2 K.

Conclusion

In this paper, an integrated PiN temperature sensor 4H-SiC GTO structure compatible with the junction termination process is simulated using TCAD simulation software. The effect of sensitivity and linearity of the sensor at different operating currents was simulated, its sensitivity was maximized to 1.64 mV/K and linearity was maximized to 0.99891. The device was simulated using a switching circuit to analyze the changes in carrier and temperature distributions at different stages of operation to analyze and compare sensor measurements, the results show that the sensor is able to monitor the temperature change of SiC GTO throughout the switching cycle in real time, measurement errors do not exceed 2K, realizing the goal of integrating a temperature sensor in the GTO. The structure monitors the temperature inside the device can avoid the generation of thermal failure which have a better development prospect.

References

[1] Yarlagadda V, Karthika G A, Nagajyothi M, Bhavani J 2022 DSTATCOM based Closed Loop Controlled Wind Power Plant with Self Excited Induction Generator for Controlling Terminal Voltage against Load Disturbances p1-6.

[2] Yamada H, Sampei M, Kashiwazaki H, Tanaka C, Takahashi T, Horiuchi T 1990 IEEE Transactions on Power Delivery 5 1327.

[3] Schrock J A, Hirsch E A, Lacouture S, Kelley M D, Bilbao A V, Ray W B, Bayne S B, Giesselmann M, Brien H O, Ogunniyi A 2016 IEEE Transactions on Power Electronics 31 8058.

[4] Geil B R, Bayne S B, Ibitayo D, Koebke M G 2005 IEEE Transactions on Plasma Science 33 1226.

[5] Li J, Pang L, Chen X, Zhang K, Wang X, Zhang Q 2021 Dianwang Jishu/Power System Technology 45 4941.

[6] Matthus C D, Erlbacher T, Hess A, Bauer A J, Frey L 2017 IEEE Transactions on Electron Devices 64 3399.

[7] Rao S, Pangallo G, Della Corte F G 2015 IEEE Electron Device Letters 36 1205.

[8] Galeckas A, Linnros J, Grivickas V, Lindefelt U, Hallin C 1997 Applied Physics Letters 71 3269.

[9] Canali C, Majni G, Minder R, Ottaviani G 1975 IEEE Transactions on Electron Devices 22 1045.

[10] Matsuura H 2002 Materials Science Forum 389-393 679.

[11] Ruff M, Mitlehner H, Helbig R 1994 IEEE Transactions on Electron Devices 41 1040.

[12] Callen H B, Scott H L 1998 American Journal of Physics 66 164.

[13] Gu H, Zhang Y, Li J, Tang Y, Bai Y 2018 14th IEEE International Conference on Solid-State and Integrated Circuit Technology (ICSICT), 31 Oct.-3 Nov. 2018 p1-3.

[14] Rao S, Di Benedetto L, Pangallo G, Rubino A, Bellone S, Della Corte F G 2016 IEEE Sensors Journal 16 6537.